Disruption of tumor suppressor gene *Hint1* leads to remodeling of the lipid metabolic phenotype of mouse liver[S]

Diren Beyoğlu,* Kristopher W. Krausz,† Juliette Martin,* Olivier Maurhofer,* Juliane Dorow,§ Uta Ceglarek,§ Frank J. Gonzalez,† Jean-François Dufour,* and Jeffrey R. Idle[1,*,†]

Hepatology Research Group,* Department of Clinical Research, University of Bern, Switzerland; Laboratory of Metabolism,† Center for Cancer Research, National Cancer Institute, National Institutes of Health, Bethesda, MD; and Institute of Laboratory Medicine,§ Clinical Chemistry and Molecular Diagnostics, University Hospital Leipzig, Leipzig, Germany

Abstract A lipidomic and metabolomic investigation of serum and liver from mice was performed to gain insight into the tumor suppressor gene *Hint1*. A major reprogramming of lipid homeostasis was found in both serum and liver of *Hint1*-null (*Hint*$^{-/-}$) mice, with significant changes in the levels of many lipid molecules, as compared with gender-, age-, and strain-matched WT mice. In the *Hint1*$^{-/-}$ mice, serum total and esterified cholesterol were reduced 2.5-fold, and lysophosphatidylcholines (LPCs) and lysophosphatidic acids were 10-fold elevated in serum, with a corresponding fall in phosphatidylcholines (PCs). In the liver, MUFAs and PUFAs, including arachidonic acid (AA) and its metabolic precursors, were also raised, as was mRNA encoding enzymes involved in AA de novo synthesis. There was also a significant 50% increase in hepatic macrophages in the *Hint1*$^{-/-}$ mice. Several hepatic ceramides and acylcarnitines were decreased in the livers of *Hint1*$^{-/-}$ mice. The changes in serum LPCs and PCs were neither related to hepatic phospholipase A2 activity nor to mRNAs encoding lysophosphatidylcholine acetyltransferases 1-4. The lipidomic phenotype of the *Hint1*$^{-/-}$ mouse revealed decreased inflammatory eicosanoids with elevated proliferative mediators that, combined with decreased ceramide apoptosis signaling molecules, may contribute to the tumor suppressor activity of *Hint1*.—Beyoğlu, D., K. W. Krausz, J. Martin, O. Maurhofer, J. Dorow, U. Ceglarek, F. J. Gonzalez, J-F. Dufour, and J. R. Idle. **Disruption of tumor suppressor gene *Hint1* leads to remodeling of the lipid metabolic phenotype of mouse liver. *J. Lipid Res.* 2014.** 55: **2309–2319.**

Supplementary key words lipidomics • metabolomics • mass spectrometry • carcinogenesis • cholesterol • phospholipids • eicosanoids • proliferation • apoptosis

This work was supported by a grant from Imperial Tobacco Limited, UK (D.B., J.R.I.), by National Institutes of Health/National Institute of Allergy and Infectious Diseases grant U19 AI067773-08/09/10 (J.R.I.), by Swiss National Science Foundation grant no. 140930 (J.F.D.), by the Bernerische und Schweizerische Krebsliga, Sasella Foundation and the Hassan Badawi Foundation Against Liver Cancer (J.R.I., J.F.D.), and by the National Cancer Institute Intramural Research Program (K.W.K., F.J.G.)

Manuscript received 6 May 2014 and in revised form 1 September 2014.

Published, JLR Papers in Press, September 5, 2014
DOI 10.1194/jlr.M050682

Tumor suppressor genes (TSGs) can be regarded as negative regulators of the cell signaling pathways that drive the growth of carcinoma (1). For hepatocellular carcinoma (HCC), for example, the activity of around 20 TSGs was reported to be lost (1–4), both by mutation (1) and by hypermethylation of promoter CpG islands (1, 3–5). One such TSG is the histidine triad nucleotide binding protein 1 (*HINT1*) gene, an ancient gene of largely unknown physiological function that leads to a variety of tumors when disrupted in mice (6–8), with evidence suggesting that it is also a human TSG (3, 9). Research has focused on the consequences of TSG inactivation on cell signaling pathways in the liver. However, little, if anything, is known about the effects of inactivation of *HINT1* and other TSGs on the hepatic metabolome and lipidome, which is surprising given the growing recognition of the role played by small metabolites (10, 11) and lipids (12, 13) in hepatocarcinogenesis.

A number of lipid signaling molecules deserve further consideration in relation to the modes of action of TSGs in carcinogenesis. Ceramide (CER) second messengers, which are derived from the catabolism of SMs or by de

Abbreviations: AA, arachidonic acid; CER, ceramide; COX2, cyclooxygenase 2; DG, diacylglycerol; ELVOL, fatty acid elongase; FADS, fatty acid desaturase; HCC, hepatocellular carcinoma; HINT1, histidine triad nucleotide binding protein 1; LPA, lysophosphatidic acid; LPC, lysophosphatidylcholine; LPCAT, lysophosphatidylcholine acyl transferase; MRM, multiple reaction monitoring; MSD, mass-selective detector; OPLS-DA, orthogonal projection to latent structures-discriminant analysis; PC, phosphatidylcholine; PCA, principal components analysis; PKC, protein kinase C; PLA2, phospholipase A2; QPCR, real-time quantitative PCR; PGE2, prostaglandin E2; PLA2, phospholipase A2; Rt, retention time; TSG, tumor suppressor gene; UPLC, ultraperformance liquid chromatography; UPLC-ESI-QTOFMS, ultraperformance liquid chromatography-electrospray ionization-quadrupole time-of-flight mass spectrometry.

[1]To whom correspondence should be addressed.
e-mail: jeff.idle@ikp.unibe.ch

[S] The online version of this article (available at http://www.jlr.org) contains supplementary data in the form of five tables and three figures.

novo synthesis from serine palmitoyl transferase or ceramide synthases (14), lead to the activation of downstream kinases and phosphatases that alter the phosphorylation levels of transcription factors, such as MYC, NF-κB, and RB (15). CERs can modulate apoptosis (15), cell proliferation, differentiation (16), and ER stress and senescence (17). Current opinion suggests that there are perhaps in excess of 200 CER species (17) and that CERs participate in the formation of plasma membrane rafts (18), which are involved in cell signaling and membrane trafficking (16). Regarding mediation of TSG activity, CERs were reported to regulate the TSG phosphatase PTEN in membrane rafts (19). Moreover, p53 downregulates sphingosine kinase 1, which may compete with ceramide synthase for the metabolism of sphingosine, thus leading to increased CER synthesis (20). Nothing is known regarding the effect of the TSG *HINT1* on CER and sphingolipid metabolism.

Lysophosphatidic acid (LPA) species act as autocrine/paracrine signaling molecules via their plasma membrane G-protein-coupled LPA receptors (21–23), which trigger many cell signaling cascades, leading to cell proliferation, migration, and differentiation (22, 23). LPAs are extracellular and intracellular molecules that are synthesized from their corresponding lysophosphatidylcholine (LPC) precursors by a secreted lysophospholipase D (24) known as autotaxin (23, 25). The relationship between LPAs and TSGs is poorly understood, except for the interaction of p53 and LPA in the regulation of hypoxia-inducible factor 1α (26). Similarly, little is known regarding the interactions between LPCs and TSGs, with the exception that 1-palmitoyl-*sn*-glycero-3-phosphocholine [LPC(16:0)] can trigger apoptosis in hepatocytes in a p53-dependent fashion (27). LPCs are also proinflammatory and may act through the induction of cyclooxygenase 2 (COX2) (28).

To shed further light on the functioning of *Hint1* in relation to its activity as a TSG, a comprehensive metabolomic and lipidomic investigation of the *Hint1*$^{-/-}$ mouse and gender-, age-, and strain-matched WT controls was undertaken. These studies show that a major reprogramming of lipid metabolism occurred in the liver when the *Hint1* gene was disrupted, an effect also detectable in serum. The net outcome was an increase in LPCs and mitogenic LPAs, together with a shift away from proapoptotic CERs and inflammatory eicosanoids in the *Hint1*$^{-/-}$ mouse.

MATERIALS AND METHODS

Animals

All mice used in this study were of the 129SvJ strain. *Hint1*-null (*Hint1*$^{-/-}$) mice were obtained from Weinstein and colleagues, who developed this mouse line (7). They were continuously bred at EPFL, Lausanne and maintained in our facility. Control WT (*Hint1*$^{+/+}$) 129SvJ mice were also maintained in our facility and cohoused with the 129SvJ/*Hint1*$^{-/-}$ mice. Animals were housed with a 12-h light/dark cycle and provided with mouse chow and water ad libitum. Experimental animal procedures complied with the National Institutes of Health *Guide for the Care and Use of Laboratory Animals* and were approved by local regulatory authorities. For metabolomic and lipidomic investigations, serum and liver tissue were obtained from 9-week-old male *Hint1*$^{+/+}$ (n = 6) and *Hint1*$^{-/-}$ (n = 6) mice between 8:00 AM and 12:00 PM under fed conditions and transported frozen on dry ice to Bethesda for analysis.

Chemicals

Palmitic (16:0), heptadecanoic (17:0) (internal standard), stearic (18:0), oleic (18:1), α-linoleic (18:2n-6), γ-linolenic (18:3), dihomo-γ-linolenic (20:3n-6), arachidonic (20:4n-6), eicosapentaenoic (20:5), and docosahexaenoic (22:6) acids were obtained from Sigma-Aldrich (Buchs, Switzerland). The following phospholipids and sphingomyelins were obtained from Avanti Polar Lipids (Alabaster, AL): lysophosphatidylcholines LPC(18:2), LPC(20:4), LPC(22:6), and LPC(17:0) (internal standard); phosphatidylcholines (PCs) PC(18:2/18:2), PC(16:0/20:4), PC(16:0/18:2), PC(18:0/18:2), PC(20:4/20:4), PC(22:6/22:6), and PC(17:0/17:0) (internal standard); lysophosphatidic acids LPA(16:0), LPA(18:0), LPA(18:1), and LPA(20:4); and SM(d18:1/16:0) and SM(d18:1/18:1). Inorganic reagents were of the highest possible grade, and solvents used were HPLC grade.

Determination of serum cholesterol and triglyceride concentrations

Serum cholesterol/cholesteryl esters and triglycerides were quantitated using BioVision kits (K603-100, K622-100, respectively; LuBioScience GmbH, Luzern, Switzerland) according to the manufacturer's instructions.

Untargeted metabolomics and lipidomics and targeted quantitative methods

For serum metabolomics, serum samples were diluted 20-fold with 66% aqueous acetonitrile containing 10 μM chlorpropamide (Sigma-Aldrich) as internal standard, vortexed, microfuged at 18,000 *g* for 20 min, and transferred to ultraperformance liquid chromatography (UPLC) injection vials. Samples were analyzed by UPLC-electrospray ionization-quadrupole time-of-flight mass spectrometry (UPLC-ESI-QTOFMS) using an Acquity BEH C18 1.7 μm (2.1 × 50 mm) column (Waters Corp., Milford, MA) under the following conditions: solvent A, 0.1% aqueous formic acid; solvent B, 0.1% formic acid in acetonitrile; 95% solvent A for 0.5 min, to 40% solvent A at 4 min, to 1% solvent A at 8 min, flushed for 1 min, then equilibrated at initial conditions for 1.5 min using a Waters Acquity UPLC. Flow rate was 0.5 ml/min, and column temperature was maintained at 60°C. Mass spectrometry on UPLC eluates was conducted in positive (ESI+) and negative (ESI−) modes using a Waters Synapt HDMS QTOFMS, scanning 50–1,000 amu at a rate of 3.3 scans/s. Capillary voltage was 3 kV, source temperature was 120°C, sampling cone was 30V, and desolvation gas (nitrogen) flow was 850 l/h at 400°C. Total run time was 10 min. Samples were randomized and included multiple pooled samples, blanks, and a standard mixture to monitor instrument stability.

For serum lipidomics, to serum (20 μl) was added cold chloroform/methanol (2:1 v/v; 100 μl) containing 5 μM each of LPC(17:0) and PC(17:0/17:0) as internal standards. The solution was vortexed for 30 s and stood for 5 min at room temperature, followed by additional vortexing. Samples were microfuged at 18,000 *g* for 10 min to separate the phases. Organic phase was removed and evaporated to dryness under nitrogen, and the dried samples were stored at −20°C until just before analysis, when evaporated extracts were dissolved in chloroform/methanol (1:1 v/v; 20 μl), propan-2-ol/water/acetonitrile (50:25:25 v/v; 200 μl) was added, and the solution was transferred to UPLC

injection vials. UPLC-ESI-QTOFMS analysis was conducted using a Waters Acquity CSH 1.7 μm C18 column (2.1 × 100 mm) under the following conditions: solvent A, acetonitrile/water (60:40 v/v) containing 10 mM ammonium acetate and 0.1% formic acid; solvent B, propan-2-ol/acetonitrile (90:10 v/v) containing 10 mM ammonium acetate and 0.1% formic acid. Gradient was 60% A to 57% A at 2 min, to 50% A at 2.1 min (ballistic gradient), to 46% A at 12 min, to 30% A at 12.1 min (ballistic gradient), to 1% A at 18 min before returning to initial conditions at 18.5 min and equilibration for 2 min. Flow rate was 0.4 ml/min, and the column was maintained at 55°C. Conditions of the mass spectrometer were as above but with a run time of 18 min.

For liver lipidomics, the protocol was adapted in part from a published method (29). Accurately weighed liver samples (~50 mg) were homogenized in water-methanol (43:57 v/v) in a Precellys® 24 bead homogenizer (Bertin Corp., Rockville, MD). Chloroform [800 μl; containing 5 μM each of LPC(17:0) and PC(17:0/17:0) as internal standards] was added, and the mixture was shaken at 37°C for 30 min. Samples were microfuged at 18,000 *g* for 20 min to separate the phases. Organic phases were removed and evaporated to dryness under nitrogen, and the dried samples were stored at −20°C until just before analysis, when evaporated extracts were dissolved in chloroform/methanol (1:1 v/v; 20 μl), and propan-2-ol/water/acetonitrile (50:25:25 v/v; 200 μl) was added and transferred to UPLC injection vials. UPLC-ESI-QTOFMS was conducted as described above for serum lipidomics.

Quantitation of lipid species was performed using either multiple reactions monitoring (MRM) or parent ion scanning using a Waters Acquity UPLC coupled to a Waters Xevo TQ mass spectrometer (UPLC-ESI-TQMS). Samples were prepared as described above for serum metabolomics; however, only 5 μM LPA(17:0) was added as internal standard. A Waters Acquity BEH C18 column (2.1 × 100 mm) was used under the following conditions: solvent A, water containing 10 mM ammonium acetate and 0.1% formic acid; solvent B, acetonitrile/propan-2-ol (5:2 v:v) containing 10 mM ammonium acetate and 0.1% formic acid. Gradient was 70% A for 1 min, then linear gradient to 50% A at 3 min, to 1% A at 8 min, held until 15 min, returning to initial conditions over 1 min, and held for an additional 2 min for column equilibration. Flow rate was 0.4 ml/min, and the column was maintained at 50°C. The mass spectrometer was operated in MRM and parent ion scanning modes and, as appropriate, in ESI+ and ESI− modes. Capillary voltage was 2.2 kV, source temperature was 150°C, and desolvation gas (nitrogen) flow rate was 850 l/h at 450°C. The cone voltage and collision energy for the MRM transitions were optimally determined by the instrument's Intellistart™ software. Details of the MRM transitions are given in supplementary Table I. Calibration curves were constructed using authentic standards and the internal standards as described above. Serum concentrations of lipid species were expressed in μM and liver concentrations in mmol/mg wet liver.

To determine relative concentrations of FAs, CERs, and acylcarnitines (ACs) in liver, extracted ion chromatograms were generated in MassLynx (Waters). For FAs, charge-to-mass ratio (*m/z*) and retention time [Rt]) in ESI− mode, in all cases for the $[M\text{-}H]^-$ ions, were 16:0 (255.2325^-; 3.18 min), 18:0 (283.2637^-; 4.30 min), 18:1 (281.2481^-; 3.29 min), 18:2 (279.2324^-; 2.62 min), 18:3 (278.2246^-; not detected), 20:3 (305.2481^-; 2.89 min), 20:4 (303.2324^-; 2.46 min), 20:5 (301.2168^-; 1.92 min), and 22:6 (327.2324^-; 2.24 min). Peak areas, normalized to heptadecanoic acid (17:0) as internal standard, were used as relative concentrations for liver samples from *Hint1*$^{+/+}$ and *Hint1*$^{-/-}$ mice. Similarly, the following ions were used to estimate relative concentrations of hepatic CERs: CER(d18:1/22:1)$[M+Na]^+$ (642.576^+; 14.29 min), CER(d16:1/23:0)$[M+Na]^+$ (630.575^+; 14.50 min), CER(d18:1/22:0)$[M+Cl]^-$ (656.576^-; 14.79 min), and CER(d18:1/24:0)$[M+Na]^+$ (672.625^+; 15.33 min). Acetylcarnitine (C2-carnitine) $[M+H]^+$ (204.124^+; 0.55 min), butyrylcarnitine (C4-carnitine) $[M+H]^+$ (232.152^+; 0.60 min), palmitoylcarnitine (C16-carnitine) $[M+H]^+$ (400.343^+; 1.42 min), and stearoylcarnitine (C18-carnitine) $[M+H]^+$ (428.374^+; 2.03 min) were similarly quantitated.

For confirmation of arachidonic acid (AA) concentrations in liver, GC-MS was performed on organic extracts of weighed *Hint1*$^{+/+}$ and *Hint1*$^{-/-}$ mouse liver containing heptadecanoic acid as internal standard. Extracts were derivatized with BSTFA/TMCS (Sigma-Aldrich) to yield TMS esters as previously described (30). The Agilent GC-MS system consisted of an oven (6890N), a mass-selective detector (MSD) (5973N), and an autosampler (7683 series). The column was an Agilent J and W HP-5ms (30 m × 0.25 mm × 0.25 μm) using helium as carrier gas at 1.0 ml/min, constant flow. The inlet was ran in split mode (ratio 5:1) and maintained at 240°C. The oven conditions were as follows: the initial temperature of 125°C was held for 2 min, ramped at 5°C/min to a final temperature of 300°C, and held for 5 min. The MSD transfer line was held at 280°C. The MSD was run in scan mode (50–550 amu) with a 6 min solvent delay. Single ion chromatograms and peak areas were generated using ChemStation software. AA TMS ester (*m/z* = 361) and heptadecanoic acid TMS ester (*m/z* = 327) were eluted at 25.70 and 21.85 min, respectively. Results were expressed as peak area ratios (relative concentrations) for AA TMS ester/heptadecanoic acid TMS ester per mg wet liver.

Determination of hepatic eicosanoids by fast liquid chromatography-quadrupole linear ion-trap mass spectrometry

Frozen liver specimens from *Hint1*$^{+/+}$ (n = 6) and *Hint1*$^{-/-}$ (n = 6) mice were shipped on dry ice to Leipzig for analysis. Weighed samples were kept on ice during the extraction. Extraction solution (n-hexane/propan-2-ol, 3/2 v/v; 600 μl), internal standard solution (5 ng/ml, 50 μl) (31), and ceramic beads were added to murine liver tissue (10 mg) or calibrators (200 μl) and quality controls in Nalgene vials (Thermo) and homogenized with a Mikro-Dismembrator (Sartorius AG, Göttingen, Germany) for 1 min and 2,500 rpm. Samples were transferred into 2 ml vials, and extraction solution (600 μl) was added. Samples were incubated for 15 h at 4°C with vortexing and then centrifuged for 5 min at 10,000 *g* and 4°C. The complete supernatant was transferred into 1.5 ml vials and evaporated under a stream of nitrogen. All dried extracts were stored at −80°C. Before LC/MS/MS, the liver extracts were reconstituted in methanol/H_2O (62:38, v/v; 500 μl), vortexed for 10 min at 4°C, and centrifuged for 1 min at 10,000 *g* and 4°C. The supernatant was used for LC/MS/MS as previously described (31) using an AB Sciex 5500 QTrap mass spectrometer (Darmstadt, Germany) with ESI in negative ion mode.

Hepatic phospholipase A2 activity

Liver homogenates were analyzed for phospholipase A2 (PLA2) activity using the EnzChk® Phospholipase A2 assay kit (Life Technologies, Grand Island, NY) according to the manufacturer's instructions. Fluorescence determinations were made using a Tecan Infinite M200 multimode microplate reader (Tecan US, Inc., Morrisville, NC).

Histology and immunohistochemistry

Liver sections from all six *Hint1*$^{+/+}$ and six *Hint1*$^{-/-}$ mice were stained in duplicate with hematoxylin and eosin and scored by a histopathologist for inflammatory infiltrates, and lobular foci of more than 10 inflammatory cells (mainly lymphocytes) were scored. The presence of sinusoidal lymphocytes and hepatocel-

lular giant cells was recorded. Immunohistochemistry was performed for detection of the murine F4/80 160 kDa cell surface glycoprotein that is expressed predominantly on murine macrophages. Paraffin-embedded, formalin-fixed sections were deparaffinized and hydrated with xylol, ethanol, and then distilled water. Antigen retrieval was performed with proteinase K, followed by washing with distilled water and endogenous peroxidase quenching with 3% methanolic hydrogen peroxide, followed by washing with distilled water and blocking with 10% rabbit serum in PBS. Primary antibody incubation was conducted with F4/80 monoclonal antibody to mouse macrophages (clone BM8; BMA Biomedicals, Augst, Switzerland). Secondary antibody incubation used a polyclonal rabbit anti-rat immunoglobulin-biotinylated secondary antibody followed by incubation using the Vectastain Universal Elite ABC kit (Adipogen, Liestal, Switzerland). DAB was used as peroxidase substrate, and counterstaining was with hematoxylin.

Real-time quantitative PCR

Total RNA was extracted from liver tissues (30 mg) preserved with RNA*later* and using RNeasy columns (QIAGEN AG, Hombrechtikon, Switzerland) with an on-column digestion step as described in the manufacturer's protocol. Total RNA (2 μg) was reverse transcribed with Superscript III reverse transcriptase (Invitrogen AG, Basel, Switzerland). cDNA was added to a fast universal PCR master mix (#4352042; Applied Biosystems, Zug, Switzerland) and amplified using an Applied Biosystems 7500 Real-Time PCR system, with primers (Applied Biosystems) specific for mouse genes *Lpcat1* (Mm00461015_m1), *Lpcat2* (Mm00557141_m1), *Lpcat3* (Mm00520147_m1), *Lpcat4* (Mm01336593_m1), *Fabp1* (Mm00444340_m1), *Slc27a1* (Mm00449511_m1), *Elvol5* (Mm00506717_m1), *Fads1* (Mm00507605_m1), and *Fads2* (Mm00517221_m1). The data were analyzed according to the $2^{\Delta\Delta}$Ct method, and Ct values were normalized to 18S rRNA (Hs99999901_s1). All reactions were performed in duplicate.

Multivariate data analysis

For the UPLC-ESI-QTOFMS metabolomics/lipidomics experiments, mass spectral data were centroided and deconvoluted to generate a multivariate data matrix using MarkerLynx (Waters). Peak picking, alignment, deisotoping, and integration were performed automatically by the software and transformed into the multivariate data matrix containing aligned peak areas with matched *m/z* and Rt values. For the serum metabolomic data, the peak areas were normalized to the peak area of the internal standard chlorpropamide (ESI+ = 277.041 and ESI− = 275.024 *m/z*; Rt = 5.3 min). Data were Pareto-scaled and analyzed by unsupervised principal components analysis (PCA), followed by orthogonal projection to latent structures-discriminant analysis (OPLS-DA) using SIMCA 13 (Umetrics AB, Malmö, Sweden) comparing data from $Hint1^{+/+}$ and $Hint1^{-/-}$ samples.

Univariate statistics

Statistical analysis of groups was made using GraphPad Prism 5 (GraphPad Software, Inc., La Jolla, CA). In all cases, nonparametric Mann-Whitney U tests were used. All means are expressed ± standard deviation, including in the figures.

RESULTS

Untargeted metabolomic analysis of mouse sera was carried out to discover biomarkers associated with HINT1 expression. A clear separation of $Hint1^{+/+}$ and $Hint1^{-/-}$ sera was found in the PCA scores plots in ESI+ and ESI− modes (**Fig. 1A**). Further analysis of the data by OPLS-DA revealed loadings S-plots with positive and negative ions that were significantly elevated and depressed in the $Hint1^{-/-}$ mice relative to the $Hint1^{+/+}$ mice (Fig. 1A). Assignment of these ions is given in supplementary Table II. The overall metabolic pattern in $Hint1^{-/-}$ mice was of upregulated LPCs.

Sixteen ions corresponding to 15 lipids were found to be lower in $Hint1^{-/-}$ mice in the serum metabolomics experiment, as well as 12 in ESI+ and four in ESI− mode. Assignment of these ions is given in supplementary Table III. The overall pattern in $Hint1^{-/-}$ mice was of downregulated phosphatidylcholine (PC) and SMs in the metabolomic (Fig. 1A) and lipidomic (Fig. 1B) investigations.

Only lipidomic analysis was performed on mouse liver. In these experiments, a clear separation of WT and $Hint1^{-/-}$ liver extracts was found in the PCA scores plots in ESI+ and ESI− modes (Fig. 1C). A total of 44 ions (37 in ESI+, 7 in ESI−) were annotated as 43 upregulated lipid constituents of the $Hint1^{-/-}$ liver (supplementary Table V). These comprised one LPC, three monoacylglycerols, four FAs (linoleic, arachidonic, docosapentaenoic, and docosahexaenoic acids), 11 PCs (red symbols in Fig. 1C), and 16 diacylglycerols (DGs) (orange symbols in Fig. 1C). A total of 38 ions (30 in ESI+, 8 in ESI−) were annotated as 28 downregulated lipid constituents of the $Hint1^{-/-}$ liver (supplementary Table V). These comprised one LPC, three PCs, four SMs (green symbols in Fig. 1C), 12 phosphatidylethanolamine species, and four ceramides (blue symbols in Fig. 1C). A summary of the lipidomic and metabolomic changes in the $Hint1^{-/-}$ mouse is given in **Table 1**.

First, the hypothesis was tested that elevated serum LPC arose from increased PLA2 activity in the liver. Because LPCs are released from membrane PCs by PLA2, the total PLA2 activity of $Hint1^{+/+}$ and $Hint1^{-/-}$ liver was determined in liver homogenates. There was no statistically significant difference in PLA2 activities in the two *Hint1* genotypes. Therefore, formation of LPCs from PCs by PLA2 did not explain the large differences in serum LPCs and PCs (**Fig. 2A**) between the genotypes; nor did this explain the patterns of hepatic LPCs and PCs (Fig. 2B) observed.

Second, the hypothesis was tested that HINT1 might increase the synthesis of PC from LPC by lysophosphatidylcholine acyl transferase (LPCAT) enzymes by upregulating expression of one or more *Lpcat* genes. Quantitative PCR (QPCR) determinations of *Lpcat1*, *Lpcat2*, *Lpcat3*, and *Lpcat4* mRNAs in WT and $Hint1^{-/-}$ livers revealed no statistically significant differences in expression of any of these four *Lpcat* genes between *Hint1* genotypes.

There occurred stark differences in hepatic fatty acid concentrations for PUFAs, for AA, and for its precursors in the de novo synthesis pathway, linoleic acid (18:2n-6) and dihomo-γ-linolenic acid (20:3n-6) (**Fig. 3**). AA, 18:2n-6, and 20:3n-6 were highly statistically significantly elevated in the $Hint1^{-/-}$ livers compared with $Hint1^{+/+}$ livers. The 2-fold elevated concentration of AA was confirmed by an independent GCMS analysis, which yielded a significant 1.5-fold increase of AA in the $Hint1^{-/-}$ mice, with values

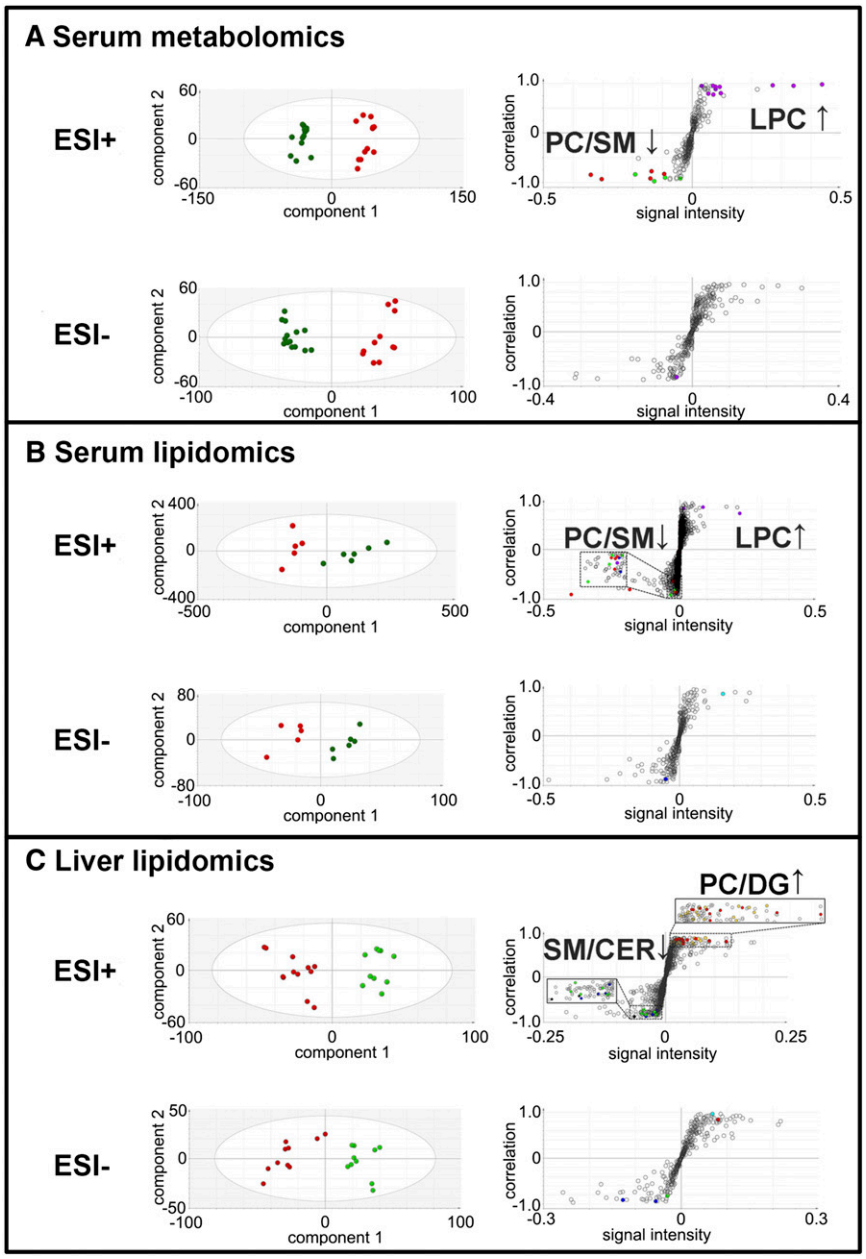

Fig. 1. Metabolomic and lipidomic analysis of serum and liver extracts in *Hint1*$^{-/-}$ (KO) and WT mice. A: Serum metabolomics, with the PCA scores plots and OPLS-DA loadings S-plots for ESI+ and ESI− modes. B: Serum lipidomics, with PCA scores plots and OPLS-DA loadings S-plots for ESI+ and ESI− modes. C: Liver lipidomics, with PCA scores plots and OPLS-DA loadings S-plots for ESI+ and ESI− modes. Green and red symbols represent WT and KO mice, respectively. In the OPLS-DA loadings S-plots, red, blue, green, orange, and purple symbols represent PC, CER, SM, DG, and LPC, respectively.

[peak area ratio (20:4/17:0)/mg liver] of 0.23 ± 0.07 and 0.15 ± 0.01 ($P = 0.02$) for *Hint1*$^{-/-}$ and *Hint1*$^{+/+}$ livers, respectively. The intermediate precursor γ-linolenic acid (18:3n-6) was not detected in livers of either genotype (Fig. 3B). Because of these metabolic findings, QPCR was conducted to evaluate mRNA expression for the three enzymes involved in the conversion of linoleic acid (18:2) to arachidonic acid (20:4). The findings for *Fads1*, *Elvol5*, and *Fads2* are given in Fig. 3B. The expression of mRNA for these three genes was 1.5- to 2-fold higher in the null mice, consistent with the observed increased hepatic AA levels. The increased hepatic levels of 18:2 and 20:4 were consistent with the observations that LPC(18:2), LPC(20:4), and PC(20:4) were also significantly higher in livers of *Hint1*$^{-/-}$ mice. It therefore appeared that one phenotype of the *Hint1*$^{-/-}$ mouse was a small (1.5- to 2-fold) accumulation of AA, together with AA metabolic precursors (Fig. 3B), and their phospholipid derivatives in the liver (Fig. 2B).

Third, because of the significantly elevated hepatic levels of AA and its phospholipid derivatives, the eicosanoid profile of *Hint1*$^{+/+}$ and *Hint1*$^{-/-}$ livers was determined using LC-ESI-TQMS. **Table 2** gives the concentrations (pg/mg liver) of 37 eicosanoids or groups of unresolved eicosanoids

TABLE 1. Summary of lipidomic changes in serum and liver for *Hint1*$^{-/-}$ mice

Serum		Liver	
↑[a]	↓	↑	↓
LPC (n = 9)[b]	LPC (n = 2)		LPC (n = 1)
LPE (n = 5)	LPE (n = 2)		
LPA (n = 4)	PC (n = 12)	PC (n = 10)	PC (n = 3)
	PE (n = 5)	PE (n = 2)	PE (n = 12)
	PE-P (n = 4)	PE-P (n = 1)	PE-P (n = 1)
	MG (n = 3)	MG (n = 3)	
DG (n = 1)	DG (n = 1)	DG (n = 17)	
	SM (n = 7)		SM (n = 3)
CER (n = 1)	CER (n = 2)	CER[c] (n = 1)	CER (n = 4)
		Sulfatide (n = 2)	
20:4[d]		18:2[d], 20:4[d], 22:5[d], 22:6[d]	
	retinylacetate		butyrylcarnitine, stearoylcarnitine, retinaldehyde, retinoic acid

LPE, lysophosphatidylethanolamine; MG, monoacylglycerol; PE, phosphatidylethanolamine; PE-P, phosphatidylethanolamine plasmalogen.

[a] ↑ and ↓ represent increases and decreases, respectively, in molecules determined by the multivariate data analysis of UPLC-ESI-QTOFMS data. The exact fold changes were not determined, except in cases where quantitation by UPLC-ESI-TQMS or extracted ion chromatograms from the UPLC-ESI-QTOFMS data were performed. Such data appear in Figs. 2, 3, and supplementary Fig. III.

[b] n is the number of molecules of a particular class that were found to be either increased or decreased in the *Hint1*$^{-/-}$ mice.

[c] Glycosylceramide (see supplementary Table IV).

[d] Fatty acid nomenclature: 18:2, linoleic acid; 20:4, arachidonic acid; 22:5, docosapentaenoic acid; 22:6, docosahexaenoic acid.

that represent 44 distinct prostaglandin and leukotriene metabolites. Contrary to expectations, prostaglandins and their metabolites were significantly lower in the null mice. Of particular note was the 4-fold decrease in hepatic PGF2α from 409 ± 142 to 101 ± 58 pg/mg liver ($P = 0.002$) and the almost 100-fold decrease in 6-keto-PGE1α from 92 ± 104 to 1 ± 0 pg/mg liver ($P = 0.01$). The only statistically significant increase observed for the null livers was the level of 20-hydroxy-PGE2 from 14 ± 4 to 114 ± 63 pg/mg liver ($P = 0.026$). This metabolite arises by the ω-hydroxylation of prostaglandin E2 (PGE2) by murine CYP4A14 (32). The downregulated eicosanoids in null livers all arose from COX1/COX2 metabolism of AA (supplementary Fig. II). Eicosanoid metabolites arising from cytochrome P450 or lipoxygenase metabolism of AA were unaltered in the null livers (Table 2), showing a degree of selectivity for the COX1/COX2 pathway.

Fourth, increased FFA uptake by the liver might explain the differences observed in hepatic fatty acids in *Hint1*$^{-/-}$ mice (33). Increased FFA hepatic uptake has been proposed as a mechanism of liver inflammation (34). However, mRNA quantitation by QPCR could not detect a difference in expression of *Slc27a1* or *Fabp1*, two genes involved in the uptake of long-chain FFA.

Fifth, representatives of two other groups of phospholipid were determined in serum of the two mouse genotypes, SMs and LPAs. There were no statistically significant differences in the serum μM concentrations of SM(d18:1/16:0) and SM(d18:1/18:1) as determined by UPLC-ESI-TQMS (Fig. 2A). Six ions corresponding to four hepatic CERs had already been observed in the lipidomic experiment to be downregulated in *Hint1*$^{-/-}$ livers (supplementary Table V). Because SMs are metabolized to proapoptotic CERs, the hepatic concentrations of these four ceramides was determined from the UPLC-ESI-QTOFMS data and expressed in arbitrary units/mg wet liver. All four CERs were statistically significantly decreased in the *Hint1*$^{-/-}$ livers, by 35% to 60% (Fig. 2C). Regarding LPAs, up to 10-fold elevated serum concentrations of LPA(16:0), LPA(18:0), LPA(18:1), and LPA(20:4) were found in *Hint1*$^{-/-}$ mice as compared with their *Hint1*$^{+/+}$ counterparts (Fig. 2A).

Sixth, because of the lipid changes observed in the livers of the null mice and the observation that C4- and C18-carnitines were depressed in the null livers (supplementary Table V), hepatic concentrations of C2-, C4-, and C18-carnitines were determined from the UPLC-ESI-QTOFMS dataset using extracted ion chromatograms for each liver sample. The results showed a highly statistically significant decrease in all three acyl carnitines, but not in C16-carnitine, in the null livers (supplementary Fig. III). This pattern is suggestive of increased fatty acid oxidation in the null mouse, but this is not supported by the hepatic fatty acid data in Fig. 3A.

Finally, because of the increase in AA, its metabolic precursors, and phospholipid metabolites in the *Hint1*$^{-/-}$ livers, we decided to examine formalin-fixed sections of WT and *Hint1*$^{-/-}$ livers for evidence of inflammation. Histological examination of liver sections from six *Hint1*$^{+/+}$ mice showed one liver with a single infiltrate with a lobular focus of 10 or more lymphocytes. The other five mice were negative in this regard. For six *Hint1*$^{-/-}$ mice, three livers were negative, but three showed 2–3 foci of lymphocytic infiltration. One of these livers displayed hepatocellular giant cells (**Fig. 4**). However, these differences were not statistically significant. In contrast, immunohistochemistry for the mouse macrophage surface glycoprotein F4/80 demonstrated a larger number of macrophages resident in the *Hint1*$^{-/-}$ liver than the *Hint1*$^{+/+}$ liver (Fig. 4A,B). The macrophage cell counts were highly statistically significantly

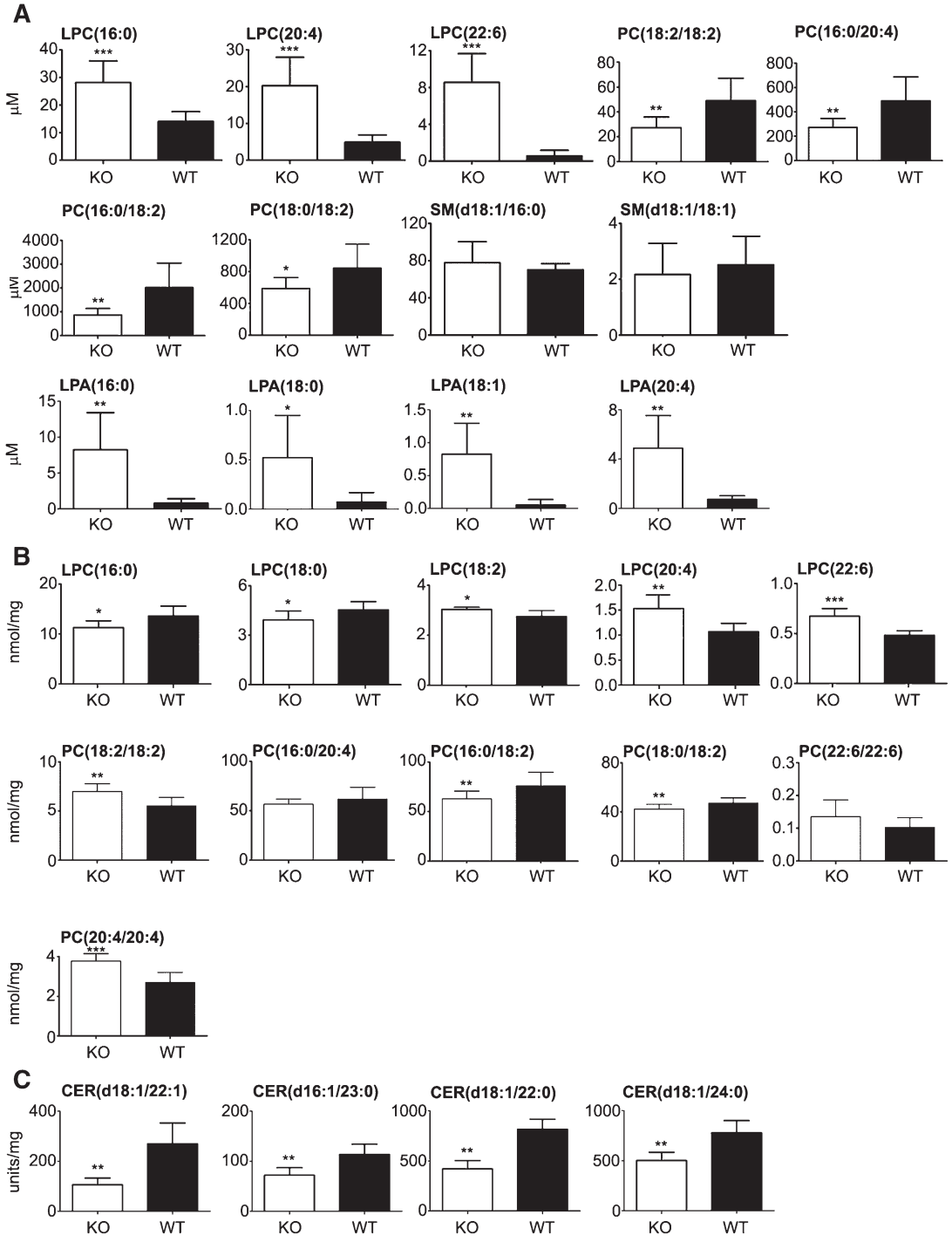

Fig. 2. Quantitation of lipids in serum of *Hint1*$^{-/-}$ (KO) and WT mice. A: Rise in serum LPC concentrations (μM), fall in serum PC concentrations and rise in serum LPA concentrations in KO mice compared with WT mice. B: Changes in hepatic phospholipids (nmol/mg wet liver) between KO mice and WT mice. C: Changes in ceramide concentrations (units/mg wet liver) between KO mice and WT mice. Analyses were performed in duplicate for WT (n = 6) and KO (n = 6) mice. * $P < 0.05$; ** $P < 0.001$; *** $P < 0.0001$.

different (Fig. 4D). Therefore, a previously undisclosed phenotype of the *Hint1*$^{-/-}$ mouse liver is an enhanced population of hepatic macrophages.

DISCUSSION

The current study revealed that the *Hint1*$^{-/-}$ mouse is characterized by a phenotype involving elevated serum LPC and LPA, with increased hepatic concentrations of AA, LPC(20:4), and PC(20:4/20:4). Precursors of de novo AA synthesis, in particular linoleic acid (18:2), were elevated. There was a decline in hepatic CERs d18:1/22:1, d16:1/23:0, d18:1/22:0, and d18:1/24:0; the C2-, C4-, and C18-acyl carnitines; and various eicosanoids derived from the COX1/COX2 pathway through PGH2. Furthermore, the *Hint1*$^{-/-}$ mouse phenotype involved expansion of the

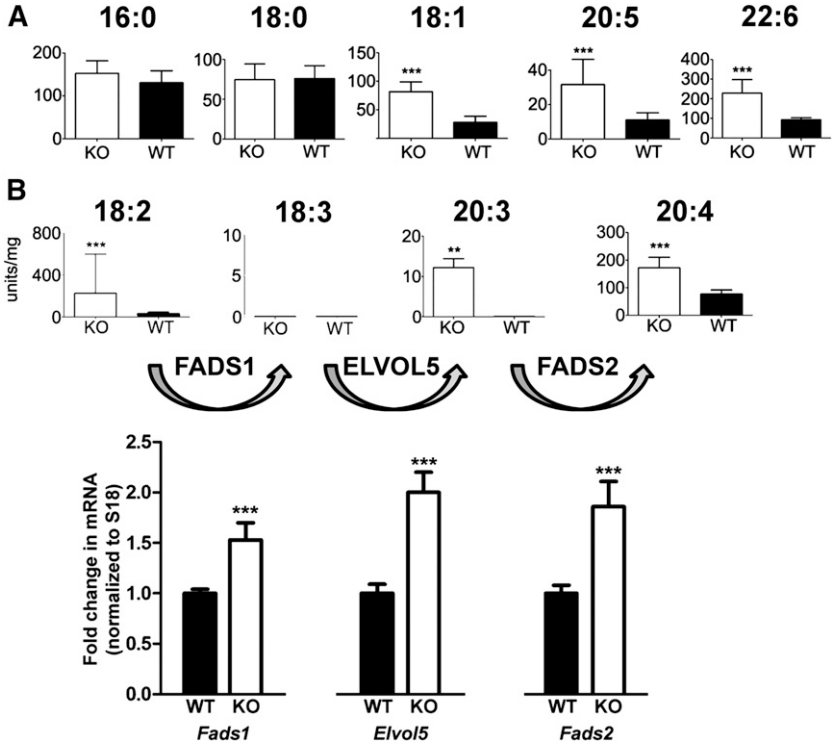

Fig. 3. Quantitation of fatty acids in liver of Hint1$^{-/-}$ (KO) and WT mice. A: No change in saturated fatty acids 16:0 and 18:0, but highly statistically significant elevations in monounsaturated (18:1) and polyunsaturated (20:5 and 22:6) essential fatty acids in KO mice compared with WT mice. Analyses were performed in duplicate for WT (n = 6) and KO (n = 6) mice. B: De novo synthesis of arachidonic acid from α-linoleic acid by desaturation and elongation in liver of KO and WT mice, showing the three enzymes involved and the fold change in mRNA expression for each of these enzymes determined by QPCR. AA and precursors are synthesized more in KO liver than in WT liver, consistent with the gene expression results.

hepatic macrophage population, presumably mostly Kupffer cells. The possible significance of these findings regarding the loss of tumor suppressor function is discussed below.

Disruption of *Hint1* increased mediators proliferative signaling in mouse liver while decreasing inflammatory eicosanoids. The prominent elevation of serum LPA concentrations into the μM range can be expected to have a significant mitogenic effect. LPAs stimulate cell surface G-protein-coupled receptors that activate multiple cell signal transduction pathways, including those involving RAS and RHO family GTPases, which regulate cell proliferation (35). LPAs are produced extracellularly from LPC by autotaxin and intracellularly from PA by PLA2 (35, 36). However, total PLA2 activity did not differ between *Hint1*$^{-/-}$ and *Hint1*$^{+/+}$ livers. Studies in hepatoma cell lines Hep3B and Huh7 have indicated that the proinflammatory cytokine TNFα promoted autotaxin expression and secretion, leading to an increase in LPA (37). Thus, inflammatory signaling within the liver, but not involving eicosanoids, might be expected to lead to LPA-directed proliferation.

Other investigations have established that the γ isotype of protein kinase C (PKCγ) was elevated in the brains of *Hint1*$^{-/-}$ relative to WT mice, with a concomitant 2-fold increase in PKC activity in *Hint1*$^{-/-}$ brain lysates (38). In addition, cytosolic PLA2, the principal form of PLA2 responsible for AA release from membrane phospholipids (39), is activated by phosphorylation by either p42 MAPK or PKC (40). Therefore, increased PKC activity in *Hint1*$^{-/-}$ liver due to the absence of a HINT1-PKC inhibitory interaction, as reported for *Hint1*$^{-/-}$ brain (38), would be expected to lead to increased cytosolic PLA2 phosphorylation, metabolic activity, and AA release. This may in part explain the increase in the AA pool observed in *Hint1*$^{-/-}$ mice. The enriched hepatic AA pool was expected to drive prostaglandin E2 (PGE2) synthesis via COX2. However, contrary to expectation, it was found that inflammatory eicosanoids were depressed in the null mouse livers. Decreased COX1/COX2 activity might lead to a backlog of AA and possibly explain the observed slight increase in hepatic AA.

Another observation of relevance was the downregulation of all PCs studied and a concomitant upregulation of all LPCs that were quantitated because several studies have reported that LPCs activate PKC (28). These observations did not appear to be due upregulated PLA2. Nor were differences detected in the expression of LPCAT genes, *Lpcat1*, *Lpcat2*, *Lpcat3*, and *Lpcat4*. Thus, an attenuated conversion of LPC to PC by LPCAT enzymes did not explain the pattern of LPCs and PCs observed. The origins of elevated serum LPCs in the *Hint1* KO mouse remain unknown.

Disruption of the *Hint1* gene may not only remove the inhibition of PKC by HINT1 but also may cause PKC to become

TABLE 2. Occurrence of eicosanoids in *Hint1*$^{+/+}$ and *Hint1*$^{-/-}$ liver

Eicosanoid	*Hint1*$^{+/+}$ (n = 6)	*Hint1*$^{-/-}$ (n = 6)	*P* (Mann-Whitney)
	pg/mg liver	*pg/mg liver*	
Tetranor-PGEM/Tetranor-PGDM	11 ± 7	16 ± 6	—
Tetranor-PGFM	58 ± 17	70 ± 22	—
20-Hydroxy-PGE2	14 ± 4	114 ± 63	0.026
20-Hydroxy-PGF2α	20 ± 9	38 ± 16	—
6-Keto-PGE1α	92 ± 104	1 ± 0	0.01
8-Iso-PGF2α	16 ± 4	10 ± 3	0.009
TxB2	97 ± 26	53 ± 30	0.026
PGF2α	409 ± 142	101 ± 58	0.002
PGF1α	35 ± 8	14 ± 6	0.002
15-Keto-PGF2α/8-Iso-PGE2/PGE2	37 ± 12	9 ± 3	0.002
8-Iso-PGE2/PGE2	54 ± 23	17 ± 5	0.015
PGE1	21 ± 5	1 ± 4	0.002
PGD2	74 ± 17	37 ± 15	0.009
15-Keto-PGE2/8-Iso-15-keto-PGE2	5 ± 1	4 ± 1	—
13,14-Dihydro-15-keto-PGF2α	15 ± 5	19 ± 10	—
5*S*,6*R*-LXA4	6 ± 1	6 ± 1	—
13,14-Dihydro-15-keto-PGE2	15 ± 5	19 ± 10	—
8-Iso-PGA2/PGA2/PGJ2	7 ± 1	9 ± 12	—
8*S*,15*S*-DiHETE	58 ± 35	84 ± 30	—
5*S*,15*S*-DiHETE	14 ± 5	34 ± 24	—
10*S*,17*S*-DiHDoHe	22 ± 13	28 ± 7	—
LTB4	21 ± 2	22 ± 3	—
Tetranor-12*S*-HETE	25 ± 10	31 ± 12	—
(±)-14,15-DHET	165 ± 60	237 ± 106	—
12*S*-HHT	603 ± 179	365 ± 224	—
(±)-11,12-DHET	60 ± 18	94 ± 42	—
(±)-8,9-DHET	40 ± 10	50 ± 14	—
5*S*,6*S*-DiHETE	n.d.	n.d.	—
19*S*-HETE	72 ± 15	53 ± 14	—
5,6-DHET	25 ± 3	28 ± 5	—
(±)-18-HETE	53 ± 12	50 ± 13	—
12*S*-HEPE	367 ± 117	381 ± 226	—
17*S*-HETE	28 ± 3	27 ± 4	—
16*S*-HETE	54 ± 14	45 ± 11	—
5*S*-HEPE	17 ± 2	19 ± 1	—
(±)-13-HODE	2,320 ± 1210	2,080 ± 738	—
(±)-9-HODE	2,710 ± 578	2,300 ± 902	—

n.d., not determined

activated. It is reported here that 16 discrete DGs were upregulated in the livers of the null mice. DGs are physiological activators of PKC and have long been considered as important second messengers in carcinogenesis (41).

CERs play an important role in apoptosis signaling. CERs also play a role in fatty acid synthesis by upregulating SREBP1c expression. In a recent report, CER(d18:1/22:0) and CER(d18:1/24:0) were two of the three most abundant CERs in human plasma (42). Both of these CERs were downregulated in serum and liver tissue of *Hint1*$^{-/-}$ mice. The principal ceramide synthase in mouse liver is CerS2, which can synthesize these two CERs (43). There are many transcriptional stimuli of ceramide synthase genes, including stress, DNA damage, and hypoxia (43). Use of the ceramide synthase inhibitor fumonisin B1 in a variety of cultured cells led to decreased CER concentrations and the inhibition of apoptosis in all cases (43). Moreover, *Cers2*-deficient mice developed hepatic adenomas, many of which progressed to HCC (44), showing that impaired specific CER synthesis can lead to HCC. Thus, the downregulation of CER serum and liver concentrations, including for CER(d18:1/22:0) and CER(d18:1/24:0), in *Hint1*$^{-/-}$ mice may partly explain the action of *Hint1* as a TSG.

The aforementioned findings are consistent with a phenotype in the *Hint1*$^{-/-}$ liver of increased proliferative signaling with reduced proapoptotic signaling. Although inflammation was shown to be required for diethylnitrosamine-induced liver cancer (45) and is thought to play a role in human HCC (46), no increase in prostaglandin inflammatory mediators was found in this study; in fact, a decrease in these molecules was observed in the livers of the null mice. It is not known which components of the lipidomic phenotype of the *Hint1*$^{-/-}$ mouse are key to cancer susceptibility in these animals. Future investigations will consolidate these findings and lead to a fuller understanding of the role played by hepatic LPC, LPA, AA, CER, DG, and macrophages in hepatocarcinogenesis in the *Hint1*$^{-/-}$ mouse. Moreover, the role played by HINT1 in the cellular physiology of the liver remains to be elucidated, but lipidomics has provided relevant new insights. As noted by Weinstein and colleagues (6), there is no other TSG that has a prokaryotic ortholog. *HINT1*, on the other hand, is highly conserved, and in the smallest genome of any cellular organism, *Mycoplasma genitalium* (580 kb), there is a homolog that shares >30% identity with the full human *HINT1* sequence (6). From the current investigations, it is clear that the HINT1 protein has a

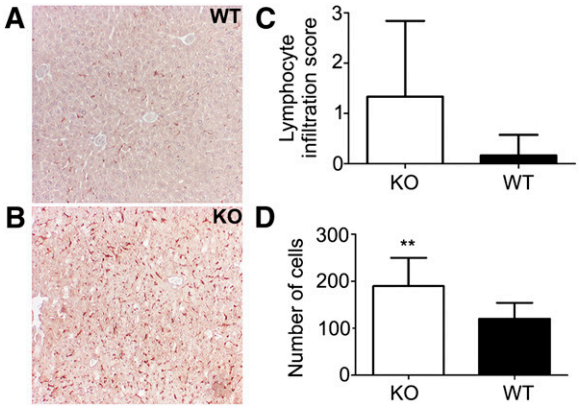

Fig. 4. Histopathology and immunohistochemistry for signs of hepatic inflammation. A: Detection of macrophages in a WT formalin-fixed liver section. Brown staining indicates macrophages. B: Detection of macrophages in a *Hint1*$^{-/-}$ formalin-fixed liver section. Brown staining indicates macrophages. C: Quantitation of lymphocyte infiltration by histopathology. D: Quantitation of F4/80 IHC for murine hepatic macrophages using three sections per liver (three sections for each of six mice per genotype). ** $P < 0.001$.

major impact on lipid homeostasis in liver and serum and, in all probability, in many other tissues. The lipid reprogramming that is associated with *Hint1* inactivation provides clues to its activity as a tumor suppressor gene.

The authors thank Dr. Gisèle Ferrand, EPFL, Lausanne, Switzerland for breeding and maintaining the *Hint1*$^{-/-}$ mice; Philipp Kellmann for immunohistochemistry studies; and Dr. Matteo Montani, Institute of Pathology, University of Bern for histology.

REFERENCES

1. Martin, J., and J. F. Dufour. 2008. Tumor suppressor and hepatocellular carcinoma. *World J. Gastroenterol.* **14:** 1720–1733.
2. Fujiwara, M., H. Marusawa, H. Q. Wang, A. Iwai, K. Ikeuchi, Y. Imai, A. Kataoka, N. Nukina, R. Takahashi, and T. Chiba. 2008. Parkin as a tumor suppressor gene for hepatocellular carcinoma. *Oncogene.* **27:** 6002–6011.
3. Revill, K., T. Wang, A. Lachenmayer, K. Kojima, A. Harrington, J. Li, Y. Hoshida, J. M. Llovet, and S. Powers. 2013. Genome-wide methylation analysis and epigenetic unmasking identify tumor suppressor genes in hepatocellular carcinoma. *Gastroenterology.* **145:** 1424–1435.
4. Yang, B., M. Guo, J. G. Herman, and D. P. Clark. 2003. Aberrant promoter methylation profiles of tumor suppressor genes in hepatocellular carcinoma. *Am. J. Pathol.* **163:** 1101–1107.
5. Tischoff, I., and A. Tannapfe. 2008. DNA methylation in hepatocellular carcinoma. *World J. Gastroenterol.* **14:** 1741–1748.
6. Li, H., Y. Zhang, T. Su, R. M. Santella, and I. B. Weinstein. 2006. Hint1 is a haplo-insufficient tumor suppressor in mice. *Oncogene.* **25:** 713–721.
7. Su, T., M. Suzui, L. Wang, C. S. Lin, W. Q. Xing, and I. B. Weinstein. 2003. Deletion of histidine triad nucleotide-binding protein 1/PKC-interacting protein in mice enhances cell growth and carcinogenesis. *Proc. Natl. Acad. Sci. USA.* **100:** 7824–7829.
8. Zhang, Y. J., H. Li, H. C. Wu, J. Shen, L. Wang, M. W. Yu, P. H. Lee, I. B. Weinstein, and R. M. Santella. 2009. Silencing of Hint1, a novel tumor suppressor gene, by promoter hypermethylation in hepatocellular carcinoma. *Cancer Lett.* **275:** 277–284.
9. Zuk, K., L. Peczek, K. Stec-Michalska, M. Medrek, and B. Nawrot. 2012. Family history of gastric cancer correlates with decreased expression of HINT1 tumor suppressor gene in gastric mucosa of dyspeptic patients. *Oncol Lett.* **3:** 219–223.
10. Beyoglu, D., and J. R. Idle. 2013. The metabolomic window into hepatobiliary disease. *J. Hepatol.* **59:** 842–858.
11. Wang, B., S. H. Hsu, W. Frankel, K. Ghoshal, and S. T. Jacob. 2012. Stat3-mediated activation of microRNA-23a suppresses gluconeogenesis in hepatocellular carcinoma by down-regulating glucose-6-phosphatase and peroxisome proliferator-activated receptor gamma, coactivator 1 alpha. *Hepatology.* **56:** 186–197.
12. Lu, D., C. Han, and T. Wu. 2012. Microsomal prostaglandin E synthase-1 promotes hepatocarcinogenesis through activation of a novel EGR1/beta-catenin signaling axis. *Oncogene.* **31:** 842–857.
13. Morales, A., M. Mari, C. Garcia-Ruiz, A. Colell, and J. C. Fernandez-Checa. 2012. Hepatocarcinogenesis and ceramide/cholesterol metabolism. *Anticancer. Agents Med. Chem.* **12:** 364–375.
14. Levy, M., and A. H. Futerman. 2010. Mammalian ceramide synthases. *IUBMB Life.* **62:** 347–356.
15. Kanzler, S., and P. R. Galle. 2000. Apoptosis and the liver. *Semin. Cancer Biol.* **10:** 173–184.
16. Chakraborty, M., and X. C. Jiang. 2013. Sphingomyelin and its role in cellular signaling. *Adv. Exp. Med. Biol.* **991:** 1–14.
17. Hannun, Y. A., and L. M. Obeid. 2011. Many ceramides. *J. Biol. Chem.* **286:** 27855–27862.
18. Castro, B. M., M. Prieto, and L. C. Silva. 2014. Ceramide: A simple sphingolipid with unique biophysical properties. *Prog. Lipid Res.* **54:** 53–67.
19. Goswami, R., D. Singh, G. Phillips, J. Kilkus, and G. Dawson. 2005. Ceramide regulation of the tumor suppressor phosphatase PTEN in rafts isolated from neurotumor cell lines. *J. Neurosci. Res.* **81:** 541–550.
20. Heffernan-Stroud, L. A., and L. M. Obeid. 2011. p53 and regulation of bioactive sphingolipids. *Adv. Enzyme Regul.* **51:** 219–228.
21. Tsujiuchi, T., M. Araki, M. Hirane, Y. Dong, and N. Fukushima. 2014. Lysophosphatidic acid receptors in cancer pathobiology. *Histol. Histopathol.* **29:** 313–321.
22. Willier, S., E. Butt, and T. G. Grunewald. 2013. Lysophosphatidic acid (LPA) signalling in cell migration and cancer invasion: a focussed review and analysis of LPA receptor gene expression on the basis of more than 1700 cancer microarrays. *Biol. Cell.* **105:** 317–333.
23. Houben, A. J., and W. H. Moolenaar. 2011. Autotaxin and LPA receptor signaling in cancer. *Cancer Metastasis Rev.* **30:** 557–565.
24. Xie, Y., and K. E. Meier. 2004. Lysophospholipase D and its role in LPA production. *Cell. Signal.* **16:** 975–981.
25. Knowlden, S., and S. N. Georas. 2014. The autotaxin-LPA axis emerges as a novel regulator of lymphocyte homing and inflammation. *J. Immunol.* **192:** 851–857.
26. Lee, S. J., Y. R. No, D. T. Dang, L. H. Dang, V. W. Yang, H. Shim, and C. C. Yun. 2013. Regulation of hypoxia-inducible factor 1alpha (HIF-1alpha) by lysophosphatidic acid is dependent on interplay between p53 and Kruppel-like factor 5. *J. Biol. Chem.* **288:** 25244–25253.
27. Kakisaka, K., S. C. Cazanave, C. D. Fingas, M. E. Guicciardi, S. F. Bronk, N. W. Werneburg, J. L. Mott, and G. J. Gores. 2012. Mechanisms of lysophosphatidylcholine-induced hepatocyte lipoapoptosis. *Am. J. Physiol. Gastrointest. Liver Physiol.* **302:** G77–G84.
28. Sevastou, I., E. Kaffe, M. A. Mouratis, and V. Aidinis. 2013. Lysoglycerophospholipids in chronic inflammatory disorders: the PLA(2)/LPC and ATX/LPA axes. *Biochim. Biophys. Acta.* **1831:** 42–60.
29. Brockmoller, S. F., E. Bucher, B. M. Muller, J. Budczies, M. Hilvo, J. L. Griffin, M. Oresic, O. Kallioniemi, K. Iljin, S. Loibl, et al. 2012. Integration of metabolomics and expression of glycerol-3-phosphate acyltransferase (GPAM) in breast cancer-link to patient survival, hormone receptor status, and metabolic profiling. *J. Proteome Res.* **11:** 850–860.
30. Fahrner, R., D. Beyoglu, G. Beldi, and J. R. Idle. 2012. Metabolomic markers for intestinal ischemia in a mouse model. *J. Surg. Res.* **178:** 879–887.
31. Kortz, L., J. Dorow, S. Becker, J. Thiery, and U. Ceglarek. 2013. Fast liquid chromatography-quadrupole linear ion trap-mass spectrometry analysis of polyunsaturated fatty acids and eicosanoids in human plasma. *J. Chromatogr. B Analyt. Technol. Biomed. Life Sci.* **927:** 209–213.
32. Ducheix, S., N. Podechard, F. Lasserre, A. Polizzi, A. Pommier, S. Murzilli, C. Di Lisio, S. D'Amore, J. Bertrand-Michel, A. Montagner, et al. 2013. A systems biology approach to the hepatic role of the

oxysterol receptor LXR in the regulation of lipogenesis highlights a cross-talk with PPARalpha. *Biochimie.* **95:** 556–567.
33. Berk, P. D., and D. D. Stump. 1999. Mechanisms of cellular uptake of long chain free fatty acids. *Mol. Cell. Biochem.* **192:** 17–31.
34. Bradbury, M. W. 2006. Lipid metabolism and liver inflammation. I. Hepatic fatty acid uptake: possible role in steatosis. *Am. J. Physiol. Gastrointest. Liver Physiol.* **290:** G194–G198.
35. Moolenaar, W. H., L. A. van Meeteren, and B. N. Giepmans. 2004. The ins and outs of lysophosphatidic acid signaling. *BioEssays.* **26:** 870–881.
36. Brindley, D. N., and C. Pilquil. 2009. Lipid phosphate phosphatases and signaling. *J. Lipid Res.* **50(Suppl):** S225–S230.
37. Wu, J. M., Y. Xu, N. J. Skill, H. Sheng, Z. Zhao, M. Yu, R. Saxena, and M. A. Maluccio. 2010. Autotaxin expression and its connection with the TNF-alpha-NF-kappaB axis in human hepatocellular carcinoma. *Mol. Cancer.* **9:** 71.
38. Varadarajulu, J., M. Lebar, G. Krishnamoorthy, S. Habelt, J. Lu, I. Bernard Weinstein, H. Li, F. Holsboer, C. W. Turck, and C. Touma. 2011. Increased anxiety-related behaviour in Hint1 knockout mice. *Behav. Brain Res.* **220:** 305–311.
39. Wick, M. J., S. Blaine, V. Van Putten, M. Saavedra, and R. A. Nemenoff. 2005. Lung Kruppel-like factor (LKLF) is a transcriptional activator of the cytosolic phospholipase A2 alpha promoter. *Biochem. J.* **387:** 239–246.
40. Nemenoff, R. A., S. Winitz, N. X. Qian, V. Van Putten, G. L. Johnson, and L. E. Heasley. 1993. Phosphorylation and activation of a high molecular weight form of phospholipase A2 by p42 microtubule-associated protein 2 kinase and protein kinase C. *J. Biol. Chem.* **268:** 1960–1964.
41. Griner, E. M., and M. G. Kazanietz. 2007. Protein kinase C and other diacylglycerol effectors in cancer. *Nat. Rev. Cancer.* **7:** 281–294.
42. Gertow, J., S. Kjellqvist, M. Stahlman, L. Cheung, J. Gottfries, O. Werngren, J. Boren, A. Franco-Cereceda, P. Eriksson, and R. M. Fisher. 2014. Ceramides are associated with inflammatory processes in human mediastinal adipose tissue. *Nutr. Metab. Cardiovasc. Dis.* **24:** 124–131.
43. Mullen, T. D., Y. A. Hannun, and L. M. Obeid. 2012. Ceramide synthases at the centre of sphingolipid metabolism and biology. *Biochem. J.* **441:** 789–802.
44. Imgrund, S., D. Hartmann, H. Farwanah, M. Eckhardt, R. Sandhoff, J. Degen, V. Gieselmann, K. Sandhoff, and K. Willecke. 2009. Adult ceramide synthase 2 (CERS2)-deficient mice exhibit myelin sheath defects, cerebellar degeneration, and hepatocarcinomas. *J. Biol. Chem.* **284:** 33549–33560.
45. Maeda, S., H. Kamata, J. L. Luo, H. Leffert, and M. Karin. 2005. IKKbeta couples hepatocyte death to cytokine-driven compensatory proliferation that promotes chemical hepatocarcinogenesis. *Cell.* **121:** 977–990.
46. Giannitrapani, L., S. Ingrao, M. Soresi, A. M. Florena, E. La Spada, L. Sandonato, N. D'Alessandro, M. Cervello, and G. Montalto. 2009. Cyclooxygenase-2 expression in chronic liver diseases and hepatocellular carcinoma: an immunohistochemical study. *Ann. N. Y. Acad. Sci.* **1155:** 293–299.